LANGMUIR

Article

Cite This: *Langmuir* 2019, 35, 3949−3962

pubs.acs.org/Langmuir

# Adsorption, Desorption, and Crystallization of Aqueous Solutions in Nanopores

Piyush Jain,[†] Olivier Vincent,[*,‡,∥] and Abraham D. Stroock[*,‡,§]

[†]Sibley School of Mechanical and Aerospace Engineering, [‡]Robert Frederick Smith School of Chemical and Biomolecular Engineering, and [§]Kavli Institute at Cornell for Nanoscale Science, Cornell University, Ithaca, New York 14853, United States

*Supporting Information*

**ABSTRACT:** Probing nanoconfined solutions in tortuous, mesoporous media is challenging because of pore size, complex pore connectivity, and the coexistence of multiple components and phases. Here, we use optical reflectance to experimentally investigate the wetting and drying of a mesoporous medium with ∼3-nm-diameter pores containing aqueous solutions of sodium chloride and lithium chloride. We show that the vapor activities (i.e., relative humidities) that correspond to optical features in the isotherms for solutions can be used to deduce the thermodynamic state of a nanoscopic solution that undergoes evaporation and crystallization upon drying and condensation and deliquescence when increasing the relative humidity. We emphasize specific equilibrium states of the system: the onset of draining during desorption and the end of filling during adsorption as well as percolation-induced scattering and crystallization. We find that theoretical arguments involving classical thermodynamics (a modified Kelvin−Laplace equation and classical nucleation theory) explain quantitatively the evolution of the optical features and thereby the state of the solution as a function of imposed vapor activity and solute concentration.

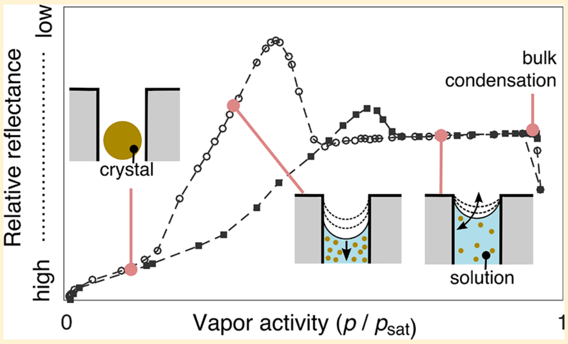

## ■ INTRODUCTION

Salt solutions frequently occupy the pore network of porous media in natural and technological contexts: the interaction of solutions with host matrixes influencing salt weathering due to stresses in the pore liquid within building materials;[1,2] the movement of contaminants in unsaturated soils leading to aquifer contamination;[3] the sequestering of $CO_2$ in brine by capillary trapping;[4] and the use of nanoporous membranes for vapor-phase desalination.[5] Wetting and drying cycles of salt solutions in porous networks regulate critical aspects in each of these contexts. The localization of crystallization during drying governs different modes of damage in materials: crystal growth upon evaporation beneath the surface results in damage due to subflorescence, while crystallization on the surface result in efflorescence-induced damage.[6,7] The transport of solutions in groundwater within the capillary fringe has been proposed to affect the solute distributions in soils; this mode of transport has implications in defining the geochemical and biological activity of groundwater systems.[8,9] However, insufficient understanding of the thermodynamics of solution-filled porous networks hinders our ability to predict and engineer in these contexts.

The influence of wetting and drying of porous media by multicomponent and multiphase fluids has been the subject of various numerical[10] and theoretical investigations.[11,12] Advances in spatiotemporal studies of water and ion transport using 3D imaging techniques such as micro-CT scanning and nuclear magnetic resonance (NMR) have aided the exploration of the local dynamics of solutions in macroporous materials.[13,14] Isotherms of porous materials using pure adsorbates are commonly used for the characterization of porous materials.[15] Also, the wetting and drying of mesoporous media presents a rich variety of effects concerning hysteresis, dynamics, and optical and acoustic signatures.[16−18] Furthermore, the shape of adsorption−desorption isotherms can be analyzed to provide insight into the dynamic and thermodynamic behavior of adsorbates under nanoconfinement and adsorbate−adsorbent interaction.[16,19] Recently, our group used reflectance isotherms to study the dynamics and thermodynamics of pure liquid water in mesoporous material and the dynamics of spatiotemporal reflectance changes as a function of imposed vapor pressure.[20]

In this article, we use reflectance isotherms of porous samples filled with aqueous solutions of various concentrations to explain, quantitatively, important characteristics of the phase behavior within the host (Figure 1a,b). We recorded changes in the reflectance of a mesoporous silicon layer filled with LiCl and NaCl solutions as a function of step increases and decreases in vapor activity, *a*, referred to as the adsorption branch (Figure 1b, filled squares) and the desorption branch (Figure 1b, open circles), respectively. We refer to these curves as reflectance isotherms (Figure 1b). We define vapor activity,

**Received:** December 28, 2018
**Revised:** February 14, 2019
**Published:** February 20, 2019

DOI: 10.1021/acs.langmuir.8b04307
*Langmuir* 2019, 35, 3949−3962

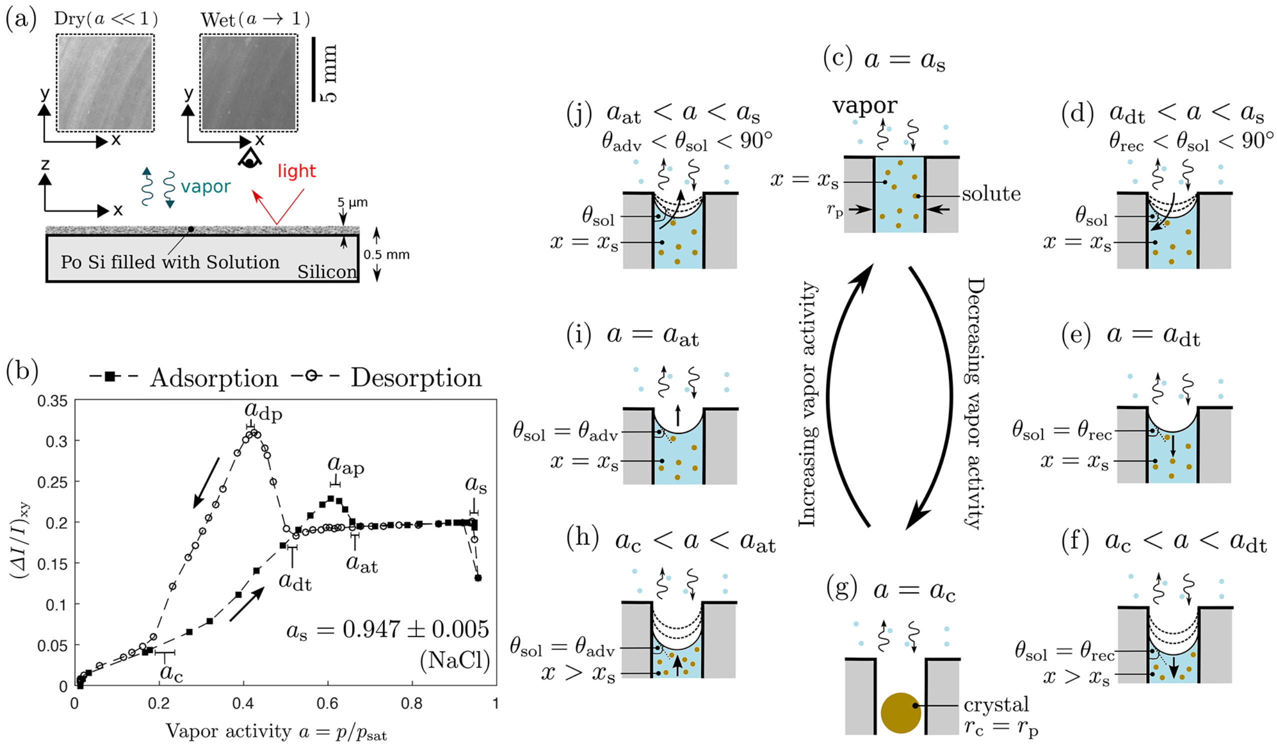

**Figure 1.** Optical reflectance isotherms of a nanoporous medium filled with an aqueous solution. (a) Optical images (top) show top views of the dry and wet states of the sample. Side-view sketch of the sample (bottom). (b) Typical reflectance isotherm (here with NaCl as the solute). (c−j) Theoretical sketches of the states of the pore solution for features noted on the isotherms in (b). The sample is entirely filled with solution at activity $a = a_s$, corresponding to the mole fraction of solute, $x_s$; the solution−vapor meniscus is flat (c). As the activity decreases, capillary pressure increases as the liquid−vapor meniscus curves (d) until $\theta_{sol} = \theta_{rec}$ as the vapor reaches the desorption-tension activity, $a_{dt}$ (e). Upon further lowering activity, desorption starts with receding menisci; the vapor pressure of receding solution decreases as the concentration of dissolved solute increases, $x > x_s$ (f), until the vapor reaches the crystallization activity, $a_c$, where supersaturation is sufficient for the critical radius of crystal nucleus, $r_c$, to be less than or equal to the pore radius, $r_p$ (g). On adsorption, the crystal deliquesces into solution, and then the pore solution reinvades with the liquid−vapor meniscus making a contact angle, $\theta_{sol} = \theta_{adv}$, with the pore wall (g) until the pore solution reaches the mouth of the pores at the adsorption-tension activity, $a_{at}$ (i). The vapor−liquid menisci relax (j), and then vapor reaches the bulk-solution activity, $a_s$, above which there is a bulk condensation of solution on the external surface. On both adsorption and desorption branches, scattering reaches maxima at vapor activities referred to as the adsorption-peak activity, $a_{ap}$, and the desorption-peak activity, $a_{dp}$.

$a = p/p_{sat}$, where $p$ is the imposed vapor pressure and $p_{sat}$ is the saturation vapor pressure of pure water at the same temperature.

Figure 1c−j presents sketches of states of the pore solution that we hypothesize are correlated with the features of interest marked on reflectance isotherms: (i) Solution completely fills the pores at the bulk-solution activity ($a_s$, Figure 1c), corresponding to the rightmost point of the isotherms. On the desorption branch (decreasing $a$), (ii) the curvature of the solution−vapor interface increases with decreasing vapor activity ($a_{dt} < a < a_s$, Figure 1d) corresponding to the plateau at high activities. (iii) The meniscus reaches its maximum curvature i.e., the tension (negative pressure) in the liquid reaches its largest magnitude and the pore liquid starts to recede into the pores at the desorption-tension activity ($a_{dt}$, Figure 1e,f), corresponding to the initial rise in $\langle \Delta I/I \rangle$ in the desorption branch (open circles in Figure 1b) of the reflectance isotherm. (iv) Crystallization in the pores occurs at the crystallization activity ($a_c$, Figure 1g), corresponding to the lower point of closure of the hysteresis loop. On the adsorption branch (increasing $a$), (v) the crystal deliquesces and the pore liquid advances to the mouth of the pores at the adsorption-tension activity ($a_{at}$, Figure 1h,i, corresponding to the upper closure point of the hysteresis loops). (vi) The curvature of the solution−vapor interface decreases with increasing vapor activity ($a_{at} < a < a_s$, Figure 1j) corresponding to the plateau on the adsorption branch until the solution completely fills the pores at the bulk-solution activity, $a_s$. As discussed in more detail in the following subsection, we interpret the peaks in both branches as being due to light scattering from heterogeneous distributions of gas-filled and liquid-filled pores. Using a single porous substrate (anodized, mesoporous silicon, pore size ∼3 nm), we collected isotherms for pure water (Figure 2), aqueous solutions of sodium chloride (NaCl, Figure 3), and aqueous solutions of lithium chloride (LiCl, Figure 4).

In this study, we analyze reflectance isotherms as a function of the amount of solute in the pore liquid to provide quantitative support for the hypotheses in Figure 1c−j. We organize the remainder of the article as follows: we describe the experimental methods for measuring the reflectance isotherms, we present theoretical equations based on classical thermodynamics to explain the evolution of features with varying activity of solution (equivalently, concentration of solution), we report and compare experimental activities with the theoretical predictions in accordance with our hypotheses, and finally, we discuss the implications of these results in our understanding of the thermodynamic state of pore solutions.

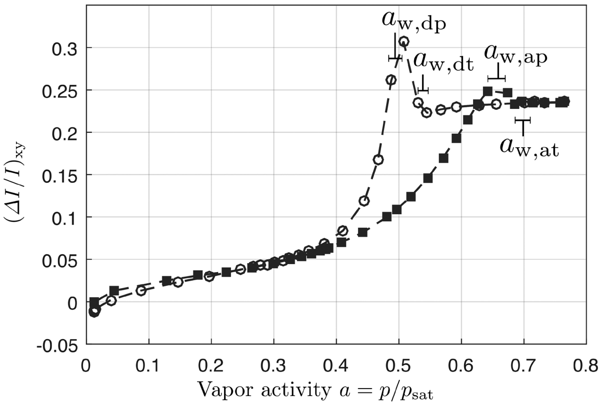

**Figure 2.** Reflectance isotherms for pure water. Adsorption-tension activity, desorption-tension activity, adsorption-peak activity, and desorption-peak activity, as defined in Figure 1, are referred to as $a_{\mathrm{w,at}}$, $a_{\mathrm{w,dt}}$, $a_{\mathrm{w,ap}}$, and $a_{\mathrm{w,dp}}$, respectively, for the special case of pure water. Closed squares and open circles represent the adsorption branch and desorption branch, respectively.

## METHODS

A mesoporous silicon layer of 5 $\mu$m thickness was formed by anodization as described previously (Figure 1a).[21] Briefly, we formed a 5-$\mu$m-thick layer of mesoporous silicon (PoSi) in the surface of a polished, p-type silicon (Si) wafer of ⟨111⟩ crystal orientation and 1−10 Ω·cm resistivity by anodization in a mixture of 1:1 49% hydrofluoric acid/pure ethanol at a current density of 20 mA/cm$^2$ for 5 min. We then thermally oxidized the substrate at 700 °C in pure oxygen for 30 s to increase the hydrophilicity and stabilize the porous layer. We expect a laterally connected pore structure with porosity $\phi = 0.45$ and a typical pore radius, $r_p$, of 1.4 nm. (The pore radius distribution is centered on 1.4 nm with a half-width at half-maximum of 0.4 nm, as estimated in previous studies from nitrogen sorption porosimetry and dynamic flow methods.[21])

Before recording reflectance isotherms for pure water, NaCl solutions, or LiCl solutions, we prepared the porous silicon sample as follows. The porous silicon substrate was sonicated in a mixture of 50% (v/v) acetone and 50% (v/v) ethanol for 5 min, and the substrate was dried with compressed nitrogen. For isotherms with pure water, the sample was then allowed to dry in vacuum for 30 min. For isotherms with solutions, a solution (1 mL) of known concentration (Figures 3 and 4) of LiCl (Alfa Aesar, 99%) or NaCl (Amresco, 99.9% biotechnology grade) was poured on porous silicon. Wettability effects (hydrophilic porous silicon vs hydrophobic surrounding bulk silicon) confined the solution to a puddle in the porosified region. The sample was allowed to imbibe the solution for 30 min. (The diffusion constant of NaCl in the aqueous phase[22] is on the order of $D \approx 10^{-5}$ m$^2$/s such that the time taken for diffusive equilibrium ($\equiv L^2/D$) of the solute in the pore liquid through the thickness, $L \approx 5$ $\mu$m, of the pores, is on the order of $\mu$s.) Excess solution on top of porous silicon was removed using a clean room wipe (Bluesorb 750, Berkshire Co.). The sample was allowed to dry in vacuum for 30 min.

We obtained reflectance isotherms (Figures 1b, 2, and 4) by placing the prepared sample (previous paragraph) in a vacuum chamber equipped with an optical window; the sample rested on the bottom surface of the chamber which was thermostated at $T = 15$ °C. Pure water vapor was obtained by evaporation from a degassed liquid water source and flowed through the chamber toward the vacuum pump. We measured the pressure of the flowing vapor, $p$ (Pa), using a pressure gauge (Pfeiffer Vacuum, CCR362) connected to the chamber. We set the pressure between $p = 0$ and $p = p_{\mathrm{sat}}$ by adjusting the relative opening of two needle valves, one upstream and one downstream from the chamber. We estimated an uncertainty in the vapor activity, $a = p/p_{\mathrm{sat}}$, of ±0.005 from the error in the pressure gauge reading and from the measured fluctuations in $T$ and $p$ during the experiments.

We started isotherms from low vapor pressure and followed the adsorption branch first. When bulk solution started to appear on the substrate surface (as evident from the sharp increase in reflected light from solution droplets on the top of the surface), we began to lower the pressure to follow the desorption branch. At each pressure step, we waited 150 s (the effective diffusion constant of water vapor in the nanopores as estimated in Vincent et al.[20] is on the order of $D \approx 10^{-10}$ m$^2$/s such that the time taken for diffusive equilibrium ($\equiv L^2/D$) of vapor through the thickness, $L \approx 5$ $\mu$m, of the pores, is only a fraction of a second) before capturing images for the next 30 s at a capture rate of 1 frame/s. Images were analyzed as described previously.[20] Briefly, we recorded time-lapse image sequences of the sample using a Point Grey Research Grasshopper3Mono camera fitted with an AF Micro-Nikkor 60 mm f/2.8D lens. We generated white-light, diffuse illumination with a Schott ACE light source (150 W halogen lamp) operating at ~50% of its maximum intensity. We analyzed the response to changes in vapor pressure by extracting the local relative change in reflectance, $(\Delta I/I)_i$, where $(\Delta I/I)_i$ was calculated by measuring the change in the grayscale value of pixels as described previously.[20] Water uptake produced a darkening of the image (images in Figure 1a), resulting in $(\Delta I/I)_i > 0$. In other words, a high $\Delta I/I$ means a dark layer (low reflectance). For the measurement of the reflectance isotherm, we evaluated the average change in intensity $\langle \Delta I/I \rangle = \frac{1}{N}\sum_i (\Delta I/I)$ over the whole region of interest (~10 mm$^2$).

We report the mean value and error of vapor activities of interest ($a_s$, $a_{\mathrm{at}}$, $a_{\mathrm{dt}}$, $a_{\mathrm{ap}}$, $a_{\mathrm{dp}}$, and $a_c$) by choosing two data points that mark the transition as defined by each of these activities in the Introduction and as shown in Figure 1b.

## THEORY

In the following section, we present a theoretical approach to interpreting how changes in vapor activity correlate to changes in the state of solutions within the porous network. We recall that our direct observations are of optical reflectance, and we discuss our interpretation of this optical information in terms of the state of the solution in the pores. To interpret the optical isotherms of the solution-filled sample (Figures 1, 3, and 4), we make comparisons to the isotherms observed with pure liquid water in the pores (Figure 2) with the same sample. In this section, we first discuss qualitatively the different regimes of the pore solution as a function of vapor activity, and then we develop expressions for the liquid−vapor equilibrium and derive relationships between the case of a solution filling the pores and the pure solvent case. Finally, after considering crystallization with a model of confined crystal nucleation in the pore solution, we discuss the origin of the peaks in scattering observed on the optical isotherms ($a_{\mathrm{dp}}$ and $a_{\mathrm{ap}}$ in Figure 1b).

**Qualitative Considerations, Assumptions, and Definitions.** Here, we elaborate qualitatively on the behavior of pores filled with solution as a function of vapor pressure before quantifying this behavior with a thermodynamic model in the next subsections.

In the following, we define the mole fraction as $x = n_s/(n_s + n_w)$, where $n_s$ is the amount of undissociated salt and $n_w$ is the amount of water. A solution with mole fraction $x$ has an equilibrium vapor pressure, $p_{\mathrm{sol}}(x) < p_{\mathrm{sat}}$, which decreases below 1 as $x$ increases above 0 as a direct consequence of solute content. We define the activity of solution as $a_{\mathrm{sol}}(x) = p_{\mathrm{sol}}(x)/p_{\mathrm{sat}} < 1$. By definition, $a_{\mathrm{sol}}(x)$ corresponds to the activity of the vapor with which a bulk sample of the solution with the same mole fraction of solute, $x$, as in the solution

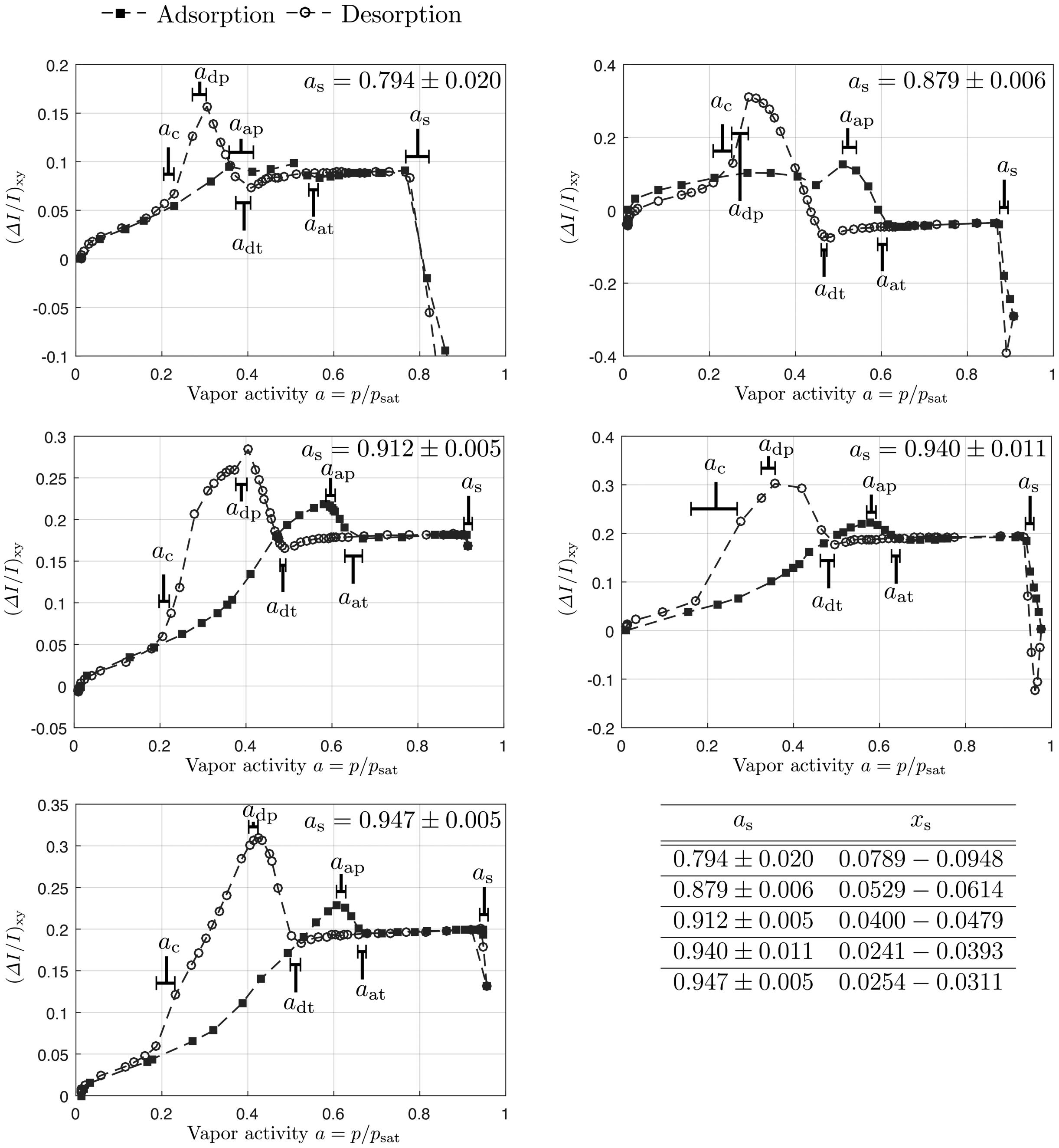

| $a_s$ | $x_s$ |
|---|---|
| $0.794 \pm 0.020$ | $0.0789 - 0.0948$ |
| $0.879 \pm 0.006$ | $0.0529 - 0.0614$ |
| $0.912 \pm 0.005$ | $0.0400 - 0.0479$ |
| $0.940 \pm 0.011$ | $0.0241 - 0.0393$ |
| $0.947 \pm 0.005$ | $0.0254 - 0.0311$ |

**Figure 3.** Reflectance isotherms for NaCl solutions at various concentrations. Concentration is measured by the bulk-solution activity, $a_s$, and corresponding mole fraction, $x_s$, as indicated in the legend. Closed squares and open circles represent adsorption branch and desorption branch, respectively. The table lists all solutions studied.

present in the pores would be in equilibrium and is thus independent of capillary pressure or confinement. The properties of solution initially used to fill the pores are denoted by the values of the molar fraction as $x_s$ (i.e., $x = x_s$) and of the corresponding activity of solution as bulk-solution activity, $a_s$ ($a_{sol}(x_s) = a_s$).

The classical picture of equilibrium between the pure pore liquid and vapor[23] involves a variation of the shape of the liquid–vapor interface as a function of vapor activity, $a = p/p_{sat}$. When $a = 1$ (vapor saturation), the meniscus is flat as in Figure 1c, while for $a < 1$, the meniscus is curved as in Figure 1d. The curvature increases when $a$ decreases, implying a varying contact angle of the interface with respect to the pore wall (Figure 1d) and a negative pressure (mechanical tension) in the liquid due to capillarity. When $a$ reaches a value at which the contact angle reaches its minimum (receding) value, equilibrium becomes impossible and the pore liquid evaporates (desorption).

If the pore is filled with solution, two important qualitative differences appear. First, vapor saturation with respect to the solution does not occur at $a = 1$ but at a value, $a_s < 1$, that decreases with increasing solute concentration; when $a = a_{sol} = a_s$, the situation is as depicted in Figure 1c, while $a < a_s$ corresponds to the varying contact angle regime of Figure 1d. Second, when the meniscus contact angle $\theta_{sol}$ reaches its receding value ($\theta_{rec}$, Figure 1e), a further decrease in the vapor

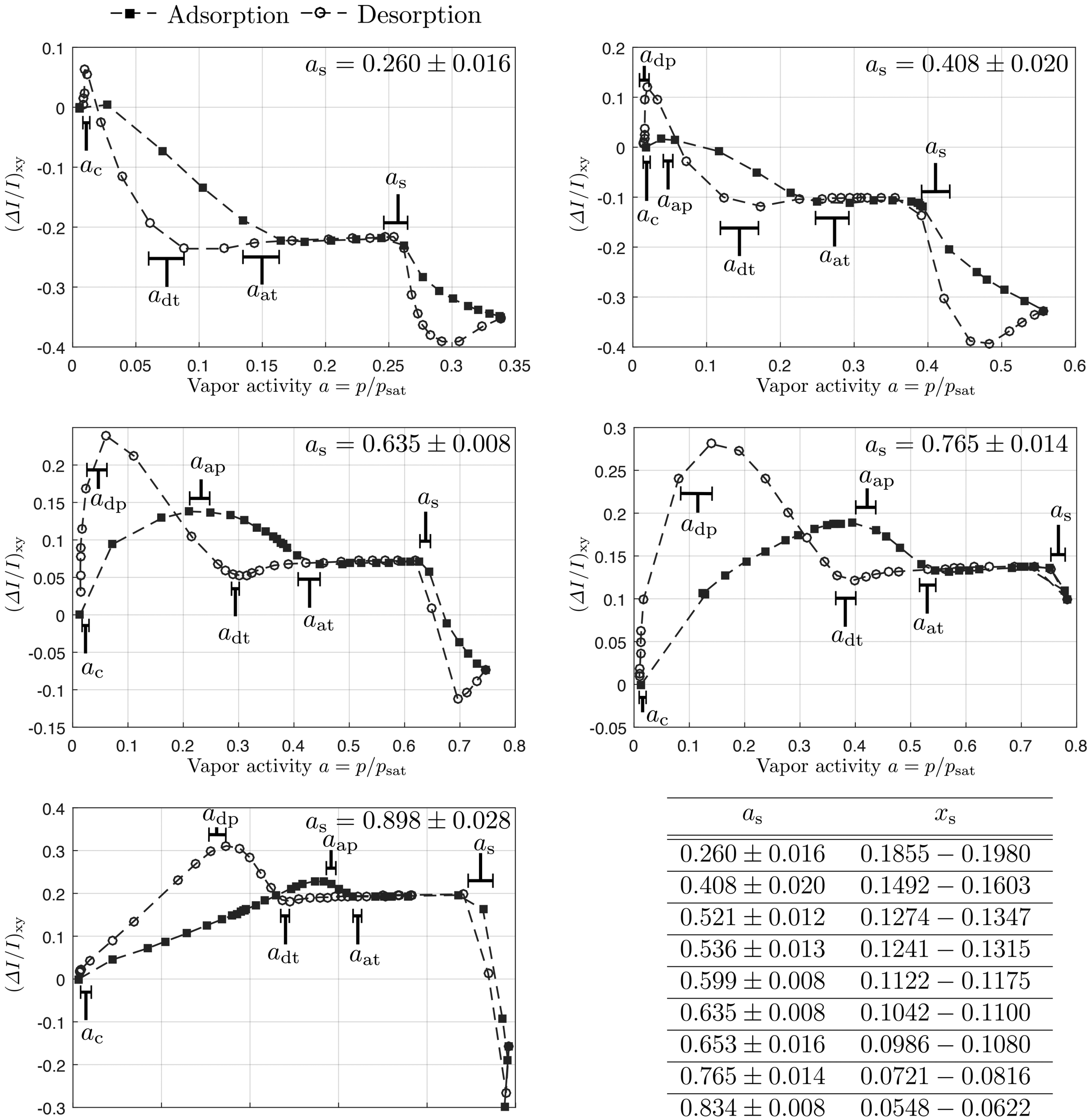

| $a_s$ | $x_s$ |
|---|---|
| $0.260 \pm 0.016$ | $0.1855 - 0.1980$ |
| $0.408 \pm 0.020$ | $0.1492 - 0.1603$ |
| $0.521 \pm 0.012$ | $0.1274 - 0.1347$ |
| $0.536 \pm 0.013$ | $0.1241 - 0.1315$ |
| $0.599 \pm 0.008$ | $0.1122 - 0.1175$ |
| $0.635 \pm 0.008$ | $0.1042 - 0.1100$ |
| $0.653 \pm 0.016$ | $0.0986 - 0.1080$ |
| $0.765 \pm 0.014$ | $0.0721 - 0.0816$ |
| $0.834 \pm 0.008$ | $0.0548 - 0.0622$ |
| $0.847 \pm 0.015$ | $0.0489 - 0.0604$ |
| $0.898 \pm 0.028$ | $0.0306 - 0.0495$ |
| $0.942 \pm 0.005$ | $0.0238 - 0.0304$ |

**Figure 4.** Examples of reflectance isotherms for LiCl solutions (SI, Figure S11) at various concentrations. Concentration is measured by the bulk-solution activity, $a_s$, and corresponding mole fraction, $x_s$, as indicated in the legend. Closed squares and open circles represent the adsorption branch and desorption branch, respectively. The table lists all solutions studied.

pressure does not induce complete evaporation of the liquid in the pore because receding of the meniscus results in an increase in the solute concentration, allowing the establishment of a new equilibrium between the solution and the vapor by lowering the chemical potential of the solvent (Figure 1f). Decreasing the vapor pressure thus results in a continuous decrease in the volume of solution in the sample until the concentration is large enough to induce the crystallization of the solute (Figure 1j).

In other words, while a pure liquid in a pore has only one degree of freedom (the contact angle with the pore wall) to achieve equilibrium with vapor, a solution has both the contact angle ($\theta_{sol}$) and concentration (mole fraction, $x$) as degrees of freedom, resulting in a larger range of possible equilibria and a more continuous evaporation process from the medium. At high vapor pressure (Figure 1d), the solution fills the pore completely, and only the contact angle varies with $a$; changes in volume induced by this change in contact angle are negligible for large enough systems so that the concentration of solute is essentially constant in that regime (varying $\theta_{sol}$, constant $x = x_s$). At lower vapor pressures (Figure 1f), another regime is reached where the volume of solution in the pore adapts to the imposed vapor pressure while the contact angle is equal to its receding value that we assume to be independent of

DOI: 10.1021/acs.langmuir.8b04307
Langmuir 2019, 35, 3949−3962

solute concentration (constant $\theta_{\mathrm{sol}}$, varying $x$). The transition between these regimes occurs at $a = a_{\mathrm{dt}}$ (Figure 1e), the desorption-tension activity at which the meniscus curvature (and thus the mechanical tension in the liquid) is maximized when decreasing the vapor pressure.

A similar transition occurs on the adsorption branch (i.e., upon increasing the vapor pressure. Following the deliquescence of the crystal, the equilibration of the confined solution with increasing vapor pressure proceeds through the dilution of the solution (Figure 1h), which expands with its advancing contact angle, $\theta_{\mathrm{adv}}$, until filling the pore completely at the adsorption-tension activity, $a_{\mathrm{at}}$ (Figure 1i)). Above $a_{\mathrm{at}}$, a regime of constant $x$ and varying $\theta_{\mathrm{sol}}$ is recovered (Figure 1j). Here, we use an elementary picture of a contact angle difference between receding ($\theta_{\mathrm{rec}}$) and advancing ($\theta_{\mathrm{adv}}$) to illustrate the basic processes at play and account in a simple manner for desorption−adsorption hysteresis; we do not attempt to model other phenomena such as pore blocking[23,24] or to investigate the physical origins of the hysteresis in our porous network. We also assume that the advancing/receding contact angles, $\theta_{\mathrm{adv(rec)}}$, do not depend on the composition of the solution and are the same for pure water ($x = 0$) and for solution (any $x$) (i.e., $\theta_{\mathrm{adv,water}} = \theta_{\mathrm{adv,solution}}$ and $\theta_{\mathrm{rec,water}} = \theta_{\mathrm{rec,solution}}$).

In the following subsection, we assume that the liquid within the pores behaves like a bulk substance with respect to solution thermodynamics and liquid−vapor equilibrium. Our previous work with liquid water in the same porous medium tends to support this assumption.[20,21] More generally, one expects only strong noncontinuum effects for pore diameters below 1 nm;[25] pore diameters in the present study are ∼3 nm. With the experiments presented here with aqueous solutions, we confront this hypothesis and find it satisfactory. While nanoscale confinement might make the pore liquid deviate from its bulk behavior, we do not resolve such effects with the measurements presented here.

**Kelvin−Laplace Relation for Pure Solvent.** We begin with a reminder of the simplest case of a pure solvent (water) in a porous medium in equilibrium with its vapor. We have previously reported on optical isotherms for pure silicon with pure water (Figure 2),[20] and this case serves as a reference to aid in the interpretation of isotherms for aqueous solutions. Throughout the article, we adopt an idealized perspective on the character of the pores: we treat them as cylindrical pores of uniform radius, $r_{\mathrm{p}}$, for the ease of subsequent derivation of capillary pressure. Equilibrium is established between bulk liquid and pure vapor at saturation pressure, $p_{\mathrm{sat}}(T)$, for a given temperature, $T$. For pure water, we use the equation of state of Wagner et al.[26] for the saturation pressure, $p_{\mathrm{sat}}(T)$. However, when the liquid in the pores is exposed to subsaturated vapor, thermodynamic equilibrium is established when the chemical potential of water, $\mu_{\mathrm{w}}^{\mathrm{liq}}$ (J/mol), in pores at pressure $P$ is equal to the chemical potential of the imposed vapor, $\mu_{\mathrm{w}}^{\mathrm{vap}}$, at pressure $p$ for a given temperature $T$

$$\mu_{\mathrm{w}}^{\mathrm{liq}}(P, T) = \mu_{\mathrm{w}}^{\mathrm{vap}}(p, T) \tag{1}$$

With the chemical potential of bulk liquid in equilibrium with vapor ($P = p = p_{\mathrm{sat}}$), $\mu_{\mathrm{o}}(T)$, as the reference, the chemical potential of pore liquid and vapor is found upon integrating the isothermal Gibbs−Duhem equation

$$\mu_{\mathrm{w}}^{\mathrm{liq}}(P, T) = \mu_{\mathrm{o}}(T) + v_{\mathrm{w}}^{\mathrm{liq}}(P - p_{\mathrm{sat}}) \tag{2}$$

and

$$\mu_{\mathrm{w}}^{\mathrm{vap}}(p, T) = \mu_{\mathrm{o}}(T) + RT \ln\left(\frac{p}{p_{\mathrm{sat}}}\right) \tag{3}$$

where $R = 8.314$ (J/K) is the universal gas constant and $v_{\mathrm{w}}^{\mathrm{liq}}$ (m$^3$/mol) is the molar volume of liquid water at temperature $T$. In eq 2, we assume $v_{\mathrm{w}}^{\mathrm{liq}}$ to be independent of pressure (i.e., the liquid is incompressible); in eq 3, we assume that the vapor is an ideal gas. Equation 1 combined with eqs 2 and 3 yield the Kelvin equation:

$$P = p_{\mathrm{sat}} + \frac{RT}{v_{\mathrm{w}}^{\mathrm{liq}}} \ln\left(\frac{p}{p_{\mathrm{sat}}}\right) \tag{4}$$

The pressure difference between the pore liquid and vapor is mechanically balanced by the capillary pressure at the liquid−vapor meniscus as given by the Young−Laplace equation

$$P - p = -\frac{2\gamma_{\mathrm{w}} \cos(\theta_{\mathrm{w}})}{r_{\mathrm{p}}} \tag{5}$$

where $\gamma_{\mathrm{w}}$ (N/m) is the surface tension at the solution−vapor interface, $\theta_{\mathrm{w}}$ is the angle the solvent makes with the pore wall, and $r_{\mathrm{p}}$ is the pore radius. In practice, the pressure, $P$, in the pore liquid, predicted by the Kelvin eq (eq 4), is much larger in magnitude ($P \approx$ MPa) than the vapor pressure or saturation vapor pressure ($p$, $p_{\mathrm{sat}} \approx$ kPa) such that eqs 4 and 5 can be rewritten, to an excellent approximation, as

$$-\frac{2\gamma_{\mathrm{w}} \cos(\theta_{\mathrm{w}})}{r_{\mathrm{p}}} = \frac{RT}{v_{\mathrm{w}}^{\mathrm{liq}}} \ln\left(\frac{p}{p_{\mathrm{sat}}}\right) = \frac{RT}{v_{\mathrm{w}}^{\mathrm{liq}}} \ln(a_{\mathrm{w}}) \tag{6}$$

In eq 6, we denote the vapor activity imposed on the sample filled with pure water as $a_{\mathrm{w}} = \frac{p}{p_{\mathrm{sat}}}$. This notation allows us to distinguish the pure solvent case from the solution case as we develop relationships between the two in the following subsections.

For the special case considered here, where the pore liquid is pure water (i.e., $a_{\mathrm{s}} = 1$), we rewrite $a_{\mathrm{at}}$ and $a_{\mathrm{dt}}$ as $a_{\mathrm{w,at}}$ ($= 0.698 \pm 0.019$) and $a_{\mathrm{w,dt}}$ ($= 0.533 \pm 0.018$), respectively (Figure 2), for clarity in subsequent derivations. In eq 6, the contact angle, $\theta_{\mathrm{w}}$, is a function of vapor activity, $a_{\mathrm{w}}$, for vapor activity $a_{\mathrm{w}} \geq a_{\mathrm{w,at}}$ on the adsorption branch and $a_{\mathrm{w}} \geq a_{\mathrm{w,dt}}$ on the desorption branch (analogous to Figure 1e,i for pure solvent). At $a = a_{\mathrm{w,at}}$ or $a = a_{\mathrm{w,dt}}$, the solvent fills the pores and the contact angle equals the equilibrium advancing angle $\theta_{\mathrm{w}} = \theta_{\mathrm{adv}}$ or the equilibrium receding angle $\theta_{\mathrm{w}} = \theta_{\mathrm{rec}}$. Hence at vapor activity, $a = a_{\mathrm{w,at(dt)}}$, eq 6 can be rewritten as

$$-\frac{2\gamma_{\mathrm{w}} \cos(\theta_{\mathrm{adv(rec)}})}{r_{\mathrm{p}}} = \frac{RT}{v_{\mathrm{w}}^{\mathrm{liq}}} \ln(a_{\mathrm{w,at(dt)}}) \tag{7}$$

We elaborated on the distinction between the advancing contact angle and the receding contact angle earlier in this section.

**Kelvin−Laplace Relation for Solutions.** Now, we adapt the same set of equations to the multicomponent case of solutions. We consider the situation as shown in Figure 1d−f,h−j where two-phase equilibrium exists between pore−solution and water vapor at temperature $T$ with the solution at pressure $P$ and water vapor at pressure $p$, respectively. Equilibrium is established when

$$\mu_w^{sol}(P, T, x) = \mu_w^{vap}(p, T) \tag{8}$$

where $\mu_w^{sol}(P, T, x)$ is the chemical potential of water in solution at pressure $P$, temperature $T$, and mole fraction $x$ and $\mu_w^{vap}(p, T)$ is the chemical potential of water vapor at pressure $p$ and temperature $T$. By integrating the isothermal Gibbs–Duhem equation with the saturation pressure of pure water, $p_{sat}(T)$, as the reference pressure and with the chemical potential of bulk pure water and vapor ($\mu_o$) as the reference, the chemical potential of liquid water in solution and vapor can be written as[27]

$$\begin{aligned}\mu_w^{sol}(P, T, x) &= \mu_o(T) + RT \ln\left(\frac{p_{sol}(x)}{p_{sat}}\right) + v_w^{sol}(P - p_{sol})\\ &= \mu_o(T) + v_w^{sol}(P - \Pi(x) - p_{sat})\end{aligned} \tag{9}$$

and

$$\mu_w^{vap}(p, T) = \mu_o + RT \ln\left(\frac{p}{p_{sat}}\right) \tag{10}$$

where $\Pi(x) = \frac{-RT}{v_w^{sol}} \ln\left(\frac{p_{sol}(x)}{p_{sat}}\right) + p_{sol} - p_{sat}$ is the osmotic pressure of the solution (assuming $v_w^{sol} \approx v_w^{liq}$),[27] $p_{sol}(x)$ is the vapor pressure of solution with dissolved mole fraction of solute $x$, and $v_w^{sol}$ (m$^3$/mol) is the molar volume of the water component of the pore solution at temperature $T$ (assuming $v_w^{sol}$ to be independent of pressure, i.e., considering the liquid to be incompressible). On defining the activity of water vapor as $a = p/p_{sat}$ (also referred to as relative humidity) and the activity of solution with dissolved mole fraction of solute $x$ as $a_{sol}(x) = p_{sol}(x)/p_{sat}$ at equilibrium, eqs 8, 9, and 10 yield

$$\begin{aligned}P &= p_{sat} + \Pi(x) + \frac{RT}{v_w^{sol}} \ln\left(\frac{p}{p_{sat}}\right)\\ &= p_{sol} + \frac{RT}{v_w^{sol}} \ln\left(\frac{p}{p_{sol}(x)}\right)\\ &= p_{sol} + \frac{RT}{v_w^{sol}} \ln\left(\frac{a}{a_{sol}(x)}\right)\end{aligned} \tag{11}$$

The pressure difference between the solution and the water vapor is again mechanically balanced by the capillary pressure at the liquid–vapor meniscus as given by Young–Laplace

$$P - p = -\frac{2\gamma_{sol}(x)\cos(\theta_{sol})}{r_p} \tag{12}$$

where $\gamma_{sol}$ (N/m) is the surface tension at the solution–vapor interface, $\theta_{sol}$, as seen in Figure 1d,j, is the equilibrium angle the solution makes with the pore wall, and $r_p$ is the pore radius. Neglecting again the solution pressure, $P$, which is much larger in magnitude ($P \approx$ MPa) than the vapor pressure or saturation vapor pressure ($p$, $p_{sat} \approx$ kPa), eqs 11 and 12 can be combined to a good approximation as

$$-\frac{2\gamma_{sol}(x)\cos(\theta_{sol})}{r_p} = \frac{RT}{v_w^{sol}} \ln\left(\frac{a}{a_{sol}(x)}\right) \tag{13}$$

We account for the concentration dependence of surface tension, $\gamma_{sol}$ (Supporting Information (SI), Figure S1), and the activity of solution, $a_{sol}$ (SI, Figures S2 and S3).

We now rewrite eq 13 to denote the two regimes elaborated on earlier in the variation in the concentration of solution with vapor activity: at high vapor pressure (Figure 1c–e,i,j), the porous medium remains full of solution and only the contact angle varies with $a = p/p_{sat}$ (constant $x$, varying $\theta_{sol}$); at low vapor pressure (Figure 1f,h), the solution recedes or advances where the concentration of solution varies with $a$ (constant $\theta_{sol}$, varying $x$).

For higher vapor activity (Figure 1c–e,i,j), the concentration of pore solution remains constant while the contact angle changes with changing vapor activity. The bulk solution (state when pores are entirely filled, Figure 1c–e,i,j) is characterized by bulk-solution activity, $a_s$ (i.e, $a_s = a_{sol}(x_s) = p_s/p_{sat}(T)$), by the vapor pressure of the bulk solution, $p_{sol}(x_s) = p_s$, and by the dissolved mole fraction of solute, $x = x_s$. Note that we calculate $x_s$ from the experimental values of bulk-solution activity, $a_s$, using empirical relations from the literature between $a_{sol}$ and $x$. (See the Supporting Information (SI) for the empirical relations.[28,29]) As described earlier, the activity of the solution, $a_s$ and the concentration of the solution, $x_s$, remain constant for the range of vapor activity as shown in Figure 1c–e,i,j, while the contact angle, $\theta_{sol}$ varies as a function of $a$. Therefore, eq 13 can be rewritten as

$$-\frac{2\gamma_{sol}(x_s)\cos(\theta_{sol})}{r_p} = \frac{RT}{v_w^{sol}} \ln\left(\frac{a}{a_s}\right) \tag{14}$$

and for the special cases of vapor activity $a = a_{at}$ and vapor activity $a = a_{dt}$, the contact angle equals the equilibrium advancing angle (i.e, $\theta_{sol} = \theta_{adv}$ (Figure 1f)) on the adsorption branch and the equilibrium receding angle (i.e, $\theta_{sol} = \theta_{rec}$ (Figure 1h)) on the desorption branch. Therefore, eq 14 can be rewritten as

$$-\frac{2\gamma_{sol}(x_s)\cos(\theta_{adv(rec)})}{r_p} = \frac{RT}{v_w^{sol}} \ln\left(\frac{a_{at(dt)}}{a_s}\right) \tag{15}$$

We use eq 15 in the next subsection to predict the evolution of $a_{at(dt)}$ with $a_s$.

For lower vapor activity ($a < a_{at}$ on the adsorption branch and $a < a_{dt}$ on the desorption branch) as shown in Figure 1f,h, the concentration of pore solution changes ($x > x_s$) while the contact angle remains constant at the equilibrium advancing angle (i.e, $\theta_{sol} = \theta_{adv}$ (Figure 1h)) on the adsorption branch and the equilibrium receding angle (i.e, $\theta_{sol} = \theta_{rec}$ (Figure 1f)) on the desorption branch. Therefore, eq 13 can be rewritten as

$$-\frac{2\gamma_{sol}(x)\cos(\theta_{adv(rec)})}{r_p} = \frac{RT}{v_w^{sol}} \ln\left(\frac{a}{a_{sol}(x)}\right) \tag{16}$$

From eq 16, we infer that for lower vapor activities ($a < a_{at}$ on the adsorption branch and $a < a_{dt}$ on the desorption branch), the concentration of the pore solution, $x$, is a function of only the imposed vapor activity and is independent of the bulk-solution activity, $a_s$ (i.e, the activity of solution when the pores are entirely filled).

**Relationship between Pure Solvent and Solution Isotherms.** Here, we derive a relation between the pure solvent and solution isotherms by combining the Kelvin–Laplace equations for pure solvent (eq 6) with that for the solution (eq 15) to predict the vapor activity associated with the onset of desorption ($a_{dt}$) and the end of adsorption ($a_{at}$). We recall that this derivation assumes an idealized case of a single pore with no noncontinuum effects. By combining eqs 7 and 15, we derive the following relation that is independent of $r_p$:

$$a_{at(dt)} = a_s \times a_{w,at(dt)}^{\gamma_{sol}(x_s) v_w^{sol}/\gamma_w v_w^{liq}} \tag{17}$$

Equation 17 serves to predict the evolution of important features noted in Figure 1b as a function of $a_s$.

We assume that the molar volume of water is independent of the concentration of solute (i.e., $v_w^{sol} \approx v_w^{liq}$),[27] and eq 17 yields

$$a_{at(dt)} = a_s \times a_{w,at(dt)}^{\gamma_{sol}(x_s)/\gamma_w} \tag{18}$$

We account for the concentration dependence of $\gamma_{sol}$ as follows: we calculate the concentration, $x_s$, from the experimental values of $a_s$ ($= a_{sol}(x_s)$) using empirical relations between $a_{sol}$ and $x$ (SI, Figures S2 and S3) and then calculate $\gamma_{sol}$ at concentration $x_s$ from the known empirical relation between $\gamma_{sol}$ and $x$ (SI, Figure S1). We highlight the effect of concentration-dependent surface tension, $\gamma_{sol}(x_s)$, by comparing it with the predicted $a_{at}$ and $a_{dt}$ upon assuming a constant surface tension ($\gamma_{sol} \approx \gamma_w$) in the SI (Figure S8).

**Classical Nucleation Theory (CNT) for Crystallization in Nanopores.** In this subsection, we adapt the theory proposed by Fukuta[30] for the freezing of a pore liquid in the context of solute crystallization. This theory accounts for the reduced pressure in the pore liquid due to metastable equilibrium with the unsaturated vapor. We consider here homogeneous salt crystallization in a supersaturated solution in a cylindrical pore, as sketched in Figure 1g. We construct this theory by hypothesizing a homogeneous mode of nucleation in order to estimate the theoretical supersaturation needed for homogeneous crystallization in a nanopore. We do not rule out the possibility of other modes of nucleation. According to CNT, for the homogeneous nucleation of a salt crystal in a supersaturated solution, there is a critical population of salt molecules that act as an embryo for crystallization. We assume that the kinetics of crystallization is fast and that crystallization is triggered as soon as the formation and growth of this critical nucleus is sterically allowable. We discuss the validity of this assumption as we discuss the results (in the Results section). The change in free energy, $\Delta G$, for the formation of a spherical crystal of radius $r$ includes contributions associated with the bulk phases (solution + crystal) and the interface between the two

$$\Delta G = \frac{\frac{4}{3}\pi r^3}{v_s^c}(\mu_{s,r_p}^c - \mu_{s,r_p}^{sol}) + 4\pi r^2 \gamma_{lc} \tag{19}$$

where $v_s^c$ (m$^3$/mol) is the molar volume of salt crystals and $\gamma_{lc}$ (J/m$^2$) is the surface tension at the interface of two phases (for NaCl, we use $\gamma_{lc} = 0.1$ J/m$^2$; for LiCl, we use $\gamma_{lc} = 0.12$ J/m$^2$);[31,32] $\mu_{s,r_p}^c$ is the chemical potential of a spherical solute crystal in a pore of radius $r_p$, and $\mu_{s,r_p}^{sol}$ is the chemical potential of dissolved solute in a pore of radius $r_p$.[33−35] Finding the maximum of $\Delta G$ with eq 19 gives the critical radius, $r_c$, in terms of chemical potential as

$$r_c = \frac{-2\gamma_{lc} v_s^c}{\mu_{s,r_p}^c - \mu_{s,r_p}^{sol}} \tag{20}$$

The activity of unsaturated vapor regulates the dissolved mole fraction, $x$, and hence the supersaturation of solution (in other words, the activities of solute and solvent) for two-phase equilibrium (eq 16). According to classical nucleation theory, a nucleus grows when the size of the nucleus is greater than the critical radius, $r_c$, and the pore radius determines the maximum size of a spherical nucleus. Hence, by employing the constraint on the size of the critical nucleus due to confinement, $r_c \leq r_p$, we can find a relationship for the theoretical mole fraction of dissolved solute needed for the onset of crystallization, $x_{c,th}$, or equivalently, the theoretical supersaturation of dissolved solute, $x_{c,th}/x_{sat}$, for the onset of crystallization from chemical and mechanical equilibrium relations substituted into eq 20 in terms of measurable and known parameters (SI)

$$r_c = r_p = \frac{2\gamma_{lc} v_s^c}{(v_s^c - v_s^{sol})\frac{2\gamma_{sol}\cos(\theta_{rec})}{r_p} + \nu RT \ln\frac{\zeta x_{c,th}}{\zeta_{sat} x_{sat}}} \tag{21}$$

where $x_{sat}$ is the mole fraction of dissolved solute in saturated bulk solution, $\zeta_{sat}$ is the activity coefficient of solute in saturated bulk solution, $\zeta$ is the activity coefficient of solute (see the definition in the SI), $\nu$ is the number of ions released upon dissociation (for both NaCl and LiCl, we take $\nu = 2$), $v_s^{sol}$ is the partial molar volume of solute in solution, and $\gamma_{sol}$ is the surface tension of the solution−vapor interface. We can rewrite eq 21 in terms of the theoretical supersaturation needed for the onset of crystallization:

$$\frac{x_{c,th}}{x_{sat}} = \frac{\zeta_{sat}}{\zeta} \exp\left[\frac{1}{\nu RT}\left(\frac{2\gamma_{lc} v_s^c}{r_p} + \frac{2\gamma_{sol}\cos(\theta_{rec})}{r_p}(v_s^{sol} - v_s^c)\right)\right] \tag{22}$$

To evaluate the properties in eq 22, we adopt the following empirical relations in terms of the mole fraction of solute ($x$): the solution vapor pressure, $p_s(x)$,[28,29] the surface tension at the solution−vapor interface, $\gamma_{sol}(x)$,[28,36] the molar volume of the solution,[28,37] and the activity coefficient of LiCl and NaCl solutions, $\zeta(x)$,[38,39] at a given temperature (SI). Here, we choose $\theta_{rec} \simeq 0°$; we show that the difference in predicted supersaturation across an experimentally reasonable range (0 to 25°) is <5%; we plot a comparison in SI Figure S9. Using this information, we solve eq 22 numerically for the value of $x_{c,th}$.

From eq 22, we infer that the onset of crystallization occurs at a fixed value of the dissolved mole fraction of the solute, $x_{c,th}$, and is independent of the initial mole fraction of the solute in the bulk pore solution, $x_s$. Because $x$ is only a function of vapor activity, $a$ (low vapor activity regime, eq 16), crystallization should be appearing at the same vapor activity $a$, independent of bulk-solution activity, $a_s$, and $x_s$.

The first term in the exponential on the right-hand side of eq 22 accounts for the unfavorable energetics of forming a critical nucleus of radius $r_c$ due to the interfacial energy of the crystal in solution ($\gamma_{lc}$); this term appears in CNT for crystallization from a bulk solution. The second term in the exponential accounts for the impact of the capillary pressure in the pore liquid associated with the liquid−vapor interface due to equilibrium with unsaturated vapor as expressed in eq 13: for unsaturated vapor, the pressure in solution is lowered; for a positive change in the partial molar volume of the solute upon crystallization ($v_s^c > v_s^{sol}$), this reduction in pressure favors crystallization.[30] This prediction agrees with the intuitive result from Le Chatelier's principle: growing the crystal with a positive change in molar volume will tend to counteract the tension imposed on the pore liquid by equilibration with an unsaturated vapor. For LiCl, the difference in molar volume of the crystal and dissolved solute (SI, Figure S7) ($v_s^{sol} - v_s^c > 0$) opposes crystallization at lower supersaturation and favors crystallization ($v_s^{sol} - v_s^c < 0$) at higher supersaturation (Figure S7). However, for NaCl, this quantity is always favorable ($v_s^{sol} - v_s^c < 0$) for crystallization (SI, Figure S7). Note that the magnitude of this effect of the negative volume of mixing decreases with increasing supersaturation (SI Figure S7).

**Peaks in Scattering.** Here, we develop our hypothesis for the peaks observed on adsorption and desorption branches of the reflectance isotherms (Figures 1b, 3, and 4). As discussed by Page et al.[17] and other authors,[18] draining of a disordered pore network upon desorption can result in the formation of gas and liquid pockets spanning a large number of pores due to pore blocking and associated percolation effects. Close to the percolation threshold, the size, $d$, of these clusters can become comparable to the wavelength of light $\lambda_{vis}$ (Figure 7a), resulting in light scattering. A similar but typically weaker effect exists upon adsorption.[18] As in our previous work,[20] we attribute the observed peaks in $\langle \Delta I/I \rangle$, corresponding to minima in reflectance, to this percolation and scattering phenomenon; we note that we also observe here a weaker effect on condensation compared to desorption (Figures 1b and 2).

As a percolation-based phenomenon, we expect this effect to be strongly linked to the amount of filling of the network, with maximum scattering at the filling fraction corresponding to the percolation threshold. Interestingly, there is a way to estimate the filled volume fraction, $\phi$, as a function of imposed vapor activity, $a$, in our experiments.

Indeed, as discussed previously in the Theory section, lowering the vapor activity, $a$, above a pore network filled with a solution results in a progressive emptying of the pore network, as the concentration of the solution increases to maintain equilibrium with the imposed vapor pressure. As a result, any given value of $a$ during desorption corresponds to a well-defined solute fraction $x$, as expressed mathematically in eq 16. Given the total amount of solute imposed by the initial concentration (equivalently, $a_s$), a filled volume fraction can be directly estimated from $a_s$ and $a$. We expect peaks of maximum scattering (lowest reflectance) to occur at similar values of $\phi$ across experiments at different values of $a_s$.

Using the Kelvin–Laplace relation for pure solvent (eq 7) and solution (eq 16) for the case when vapor activity $a < a_{at}$ on the adsorption branch and $a < a_{dt}$ on the desorption branch, we derive a relation independent of $r_p$

$$a = a_{sol}(x) \times a_{w,at(dt)}^{\gamma_{sol}(x) v_w^{sol}/\gamma_w v_w^{liq}} \tag{23}$$

and with the same assumption as made previously (i.e, the molar volume of water is independent of the concentration of solute, $v_w^{sol} \approx v_w^{liq}$),[27] eq 23 yields

$$a = a_{sol}(x) \times a_{w,at(dt)}^{\gamma_{sol}(x)/\gamma_w} \tag{24}$$

On the adsorption branch, we denote the vapor activity at the maximum $\langle \Delta I/I \rangle$ (lowest reflectance) by $a_{ap}(<a_{at})$, referred to hereafter as the adsorption-peak activity; on the desorption branch, we use $a_{dp}(<a_{dt})$, referred to hereafter as desorption-peak activity (Figure 5). We use eq 24 to calculate the dissolved mole fraction of solute, $x = x_{ap}$ and $x = x_{dp}$, at vapor activity, $a = a_{ap}$ and $a = a_{dp}$, respectively. At adsorption-peak and desorption-peak vapor activities (i.e., $a = a_{ap}$ and $a = a_{dp}$, which are known experimentally), we denote (i) the activity of the solution as $a_{sol}(x_{ap})$ and $a_{sol}(x_{dp})$, (ii) the corresponding dissolved mole fraction of solute as $x_{ap}$ and $x_{dp}$, and (iii) the surface tension of solution as $\gamma_{sol}(x_{ap})$ and $\gamma_{sol}(x_{dp})$. Upon substituting eq 24 for the activity of solution and surface tension as a function of the dissolved mole fraction of solute, $x$, at vapor activities $a_{ap}$ and $a_{dp}$, we solve for $x_{ap}$ and $x_{dp}$ using relations implicit in $x_{ap}$ and $x_{dp}$, respectively,

$$\left(\frac{a_{ap}}{a_{sol}(x_{ap})}\right)^{1/\gamma_{sol}(x_{ap})} = a_{w,at}^{1/\gamma_w} \tag{25a}$$

$$\left(\frac{a_{dp}}{a_{sol}(x_{dp})}\right)^{1/\gamma_{sol}(x_{dp})} = a_{w,dt}^{1/\gamma_w} \tag{25b}$$

where the activity of the solution, $a_{sol}$, and the surface tension, $\gamma_{sol}$, are known as empirical functions of the dissolved mole fraction of solute, $x$ (SI). Once we have evaluated $x_{ap(dp)}$ from eq 25a and 25b, we calculate the volume fraction of liquid-filled pores, $\phi_{ap(dp)}$, corresponding to vapor activity $a = a_{ap(dp)}$, assuming that the total amount of solute remains constant during adsorption and desorption

$$\phi_{ap(dp)} = \frac{V_{ap(dp)}}{V_s} = \frac{v_{sol}(x_{ap(dp)})x_s}{v_{sol}(x_s)x_{ap(dp)}} \tag{26}$$

where $v_{sol}(x_s)$ and $v_{sol}(x_{ap(dp)})$ are the molar volume of the solutions corresponding to the dissolved mole fraction of solute being $x_s$ and $x_{ap(dp)}$, respectively.

We note that in the case of a pure fluid filling the pore network, desorption occurs in a very narrow range of vapor activity, as illustrated in Figure 2. This is contrary to the continuous character of evaporation for a solution, which is the basis of the estimate of volume fraction filling developed above. As a result, the calculations above cannot be applied to the case of pure water but only to the case of solutions.

## ■ RESULTS AND DISCUSSION

**Qualitative Features of Reflectance Isotherms.** In this subsection, we discuss qualitatively each of the noted features in Figure 1b as a function of the activity of bulk NaCl (Figure 3) and LiCl (Figure 4) solutions, $a_s$, within the pore volume. Figures 3 and 4 present reflectance isotherms for NaCl (Figure 3) and LiCl (Figure 4) solutions for a range of bulk-solution activities and corresponding mole fraction of solute for NaCl ($a_s = 0.794 \pm 0.020$–$0.947 \pm 0.005$ ($\equiv x_s = 0.0254$–$0.0948$)) and for LiCl ($a_s = 0.260 \pm 0.016$–$0.942 \pm 0.005$ ($\equiv x_s = 0.0238$–$0.1980$)). In the case of LiCl, we collected isotherms at additional, intermediate activities; we present these in Figure S11.

The reflectance isotherms for pure solvent (here, water; Figure 2) have features characteristic of mass isotherms: plateaus on both adsorption and desorption branches at higher activity ($a > a_{w,at}$ and $a > a_{w,dt}$), associated with entirely filled pores; reversible variation for lower vapor activity ($a < 0.4$), associated with molecules adsorbing on the pore walls; and hysteresis between adsorption and desorption branches in between these two reversible regimes. In addition, we observe a feature characteristic only of the reflectance isotherms, where scattering increases, or, in other words, reflectance decreases before the end of filling and the onset of draining on adsorption ($a_{w,ap}$) and desorption branches ($a_{w,dp}$), respectively. This observation is consistent with the decrease in transmission observed on adsorption and desorption branches in porous Vycor.[17,18]

Qualitatively, the reflectance isotherms for NaCl and LiCl solutions are similar to those of the pure solvent but differ in two aspects: (1) the trajectory of the desorption curve; the desorption curve, for pure solvent, falls sharply onto the adsorption curve, while for the case of solution, the desorption curve follows a more continuous and globally much wider trajectory before collapsing onto the adsorption curve (Figure 2 and Figures 3 and 4). Similarly, we observe a sharp increase in scattering for the case of pure water for the vapor activity for $a_{w,dp} < a < a_{w,dt}$, while we observe a continuous increase in scattering on the desorption branch for $a_{dp} < a < a_{dt}$. These behaviors agree with our hypothesis that, unlike for the pure solvent, the recession of solution and the associated increase in concentration (equivalently, a decrease in the activity of solution) below $a_{dt}$ allow for the continuous re-establishment of equilibrium (Figure 1f). This phenomenon allows us to determine the filling fraction of the porous media (from the corresponding solute concentration and assuming that the moles of solute remain constant) at a given vapor activity (eq 26). (2) Closure of the hysteresis loop: For pure solvent, we observe the characteristic step down in the desorption branch, leading to the closure of the hysteresis loop (Figure 2), which is attributed to various effects such as the cavitation-induced emptying of pores, pore blocking, and percolation.[15,17,40] In contrast, we observe a gradual closure of the hysteresis loop for the case of solutions. From the isotherms in Figure 3 and 4, we note that the vapor activity associated with the closure of the hysteresis loop, $a_c$, is independent of the bulk-solution activity, $a_s$, and occurs at a fixed value of vapor activity, $a$; this observation indicates that the hysteresis loop collapses at a fixed value of solute concentration (the solute concentration is only a function of vapor activity for vapor activity, $a$, lower than $a_{dt}$ and independent of the initial activity of the solution ($a_s$) or, equivalently, the initial concentration of the solution ($x_s$); see eq 16 and the Theory section), as should occur with crystallization (eq 22, Theory section). Later in this section, we explain this observation quantitatively.

We now turn to a quantitative analysis of the variation of features observed in the isotherms for solutions of NaCl (Figure 3) and LiCl (Figure 4).

**Shifts in Adsorption and Desorption as a Function of Solute Concentration.** Figure 5 presents the activities, $a_{at}$ and $a_{dt}$, extracted from the isotherms in Figures 3 and 4 as functions of $a_s$. In the same figure, we plot the predictions of the Kelvin equation for solutions with pure water as a reference based on eq 18. The theoretical prediction well matches the experimental values of $a_{at}$ and $a_{dt}$ for both LiCl (solid filled circles) and NaCl (diamonds) solutions with pure water (transparent filled circles; $a_s = 1$) as the reference point. This agreement supports the hypothesized state of solution in the pore at the vapor activities, $a_{at}$ and $a_{dt}$ (i.e., the solution is under characteristic maximum tension (negative pressure) before the end of filling and the onset of draining on the adsorption and desorption branches, respectively).

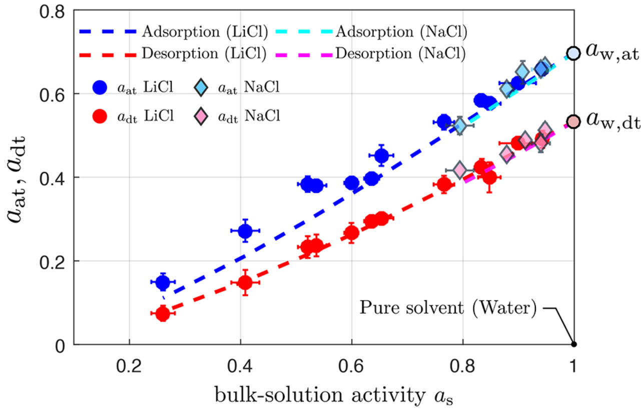

**Figure 5.** Effect of solute concentration on adsorption and desorption: adsorption-tension activity, $a_{at}$ (completion of pore filling), and desorption-tension activity, $a_{dt}$ (onset of pore emptying) from isotherms as in Figures 3 and 4. Vapor activities for solution as predicted by the Kelvin equation (eq 18) are shown by dashed lines for LiCl and NaCl solutions. Experimental values of $a_{at}$ and $a_{dt}$ from isotherms as in Figures 3 and 4 for LiCl and NaCl are shown as indicated. Adsorption-tension activity and desorption-tension activity (i.e., $a_{w,at}$ and $a_{w,dt}$), as extracted from Figure 2, are plotted as indicated. Error bars for $a_s$, $a_{at}$, and $a_{dt}$ represent the uncertainty in experimental values extracted from the isotherm (Methods section). In eq 18, the surface tension of solution as a function of NaCl and LiCl concentrations is reported in the SI (Figure S1), and the surface tension for pure water is taken to be 73.5 mN/m at 15 °C.

The agreement shown above between theoretical and experimental predictions of $a_{at}$ and $a_{dt}$ along with the hypothesized state of solution under tension at vapor activities $a_{at}$ and $a_{dt}$ (Figure 1e,i) and the hypothesized state of the no-tension condition at vapor activity, $a_s$ (Figure 1c) indicates that the same theoretical principles explain the state of solution in the pores on the adsorption plateau ($a_{at} < a < a_s$) and on the desorption plateau ($a_{dt} < a < a_s$) (Figure 1d,j). In other words, the tension in the pores at a given activity in both the adsorption plateau ($a_{at} < a < a_s$) and the desorption plateau ($a_{dt} < a < a_s$) should be given by the modified Kelvin equation (eq 11), and the pressure difference should be balanced mechanically with the varying contact angle between the liquid meniscus and the pore wall as given by the Laplace equation (eq 12, Figure 1d,j). As suggested by eq 11, the salt concentration (activity of solution or osmotic pressure) tunes the tension in nanopores for any given vapor activity. The success of our predictions also supports our assumption that bulk thermodynamic properties ($\gamma_{sol}$, $a_{sol}$) remain relevant in the pores studied here with a diameter of ~3 nm.

We also note that when increasing the vapor activity to above $a_c$, the crystal present in the pore needs to transition to a solution (a process known as deliquescence). Because we know that at the upper closure of the adsorption branch (vapor activity $a_{at}$) the pores are filled with solution, it follows that $a_{at}$ provides an upper bound for the deliquescence activity. Interestingly, for NaCl solutions, the experimental values of $a_{at}$ are well below the bulk deliquescence point of NaCl crystals at $a \approx 0.75$,[41] indicating strong confinement effects on the deliquescence point of crystals in nanopores.

**Crystallization within Pores at Large Supersaturations.** As we have noted above, the results presented in Figures 3 and 4 show that the lower closure of the hysteresis cycle of the reflectance isotherms (vapor activity, $a_c$) always occurs at similar vapor activities for a given solute, regardless of the initial concentration of that solute in the porous network. In other words, $a_c$ is independent of the bulk-solution activity $a_s$: in the case of NaCl, we have $a_c = 0.215 \pm 0.025$ for all measured isotherms (with $a_s$ varying from 0.79 to 0.95), while for LiCl, $a_c$ = 0.014 ± 0.009 (with $a_s$ varying from 0.26 to 0.94); see Figure 6a. We note that while closure for LiCl is consistent, it happens at very low vapor pressures that are at the limit of values that we can resolve with our experimental system.

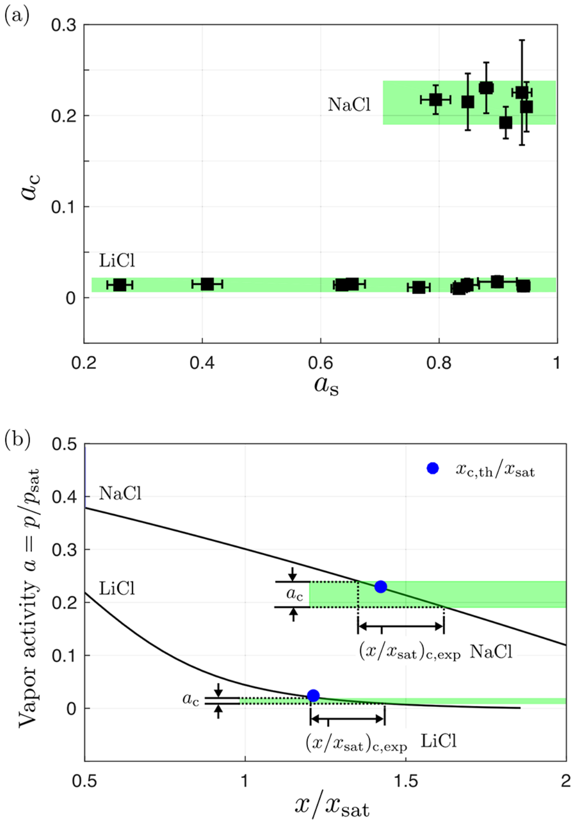

**Figure 6.** Effect of initial solute concentration on the lower closure point of the hysteresis cycles due to crystallization ($a_c$) and corresponding supersaturations. (a) Experimental values of crystallization activity ($a_c$) as a function of bulk-solution activity ($a_s$) for NaCl from isotherms as in Figure 3 and for LiCl as in isotherms from Figure 4, where $a_c$ is the lower point of closure of the adsorption and desorption branches. The shaded green region is the range given by the average of all error bars on values of $a_c$ around the average values of $a_c$. (b) Theoretical and experimental supersaturation for the crystallization of LiCl and NaCl solutions. The solid black line represents the equilibrium vapor activity vs supersaturation for $r_p$ = 1.4 nm for NaCl and LiCl solutions as indicated. The blue dots are the values of theoretical supersaturation for the onset of crystallization, $x_{c,th}/x_{sat}$, found from the classical nucleation theory for $r_c = r_p$ (eqs 21 and 22) and correspond to $r_p$ = 1.4 nm. The shaded green is the range of averaged experimental vapor activity, $a_c$ (the same as in panel a). $(x/x_{sat})_{c,exp}$ is the supersaturation associated with $a_c$ (obtained experimentally) for the onset of crystallization.

As explained in the Theory section, when the pores are not full (i.e., during desorption below $a_{dt}$ or adsorption below $a_{at}$), there is a direct relation between the imposed vapor activity, $a$, and the solute concentration in the pores (eq 16); thus, the observation of closure at constant $a_c$ suggests a process that occurs at a fixed solute concentration. In Figure 6b, we plot this relation for both NaCl and LiCl solutions (black lines), with concentration expressed in terms of the supersaturation ratio $x/x_{sat}$, where $x_{sat}$ is the mole fraction of solute in saturated solution at $T$ = 15 °C (for NaCl, $x_{sat}$ = 0.099; for LiCl, $x_{sat}$ = 0.242). These curves allow us to translate the measured values of $a_c$ (Figure 6a) into corresponding supersaturations, and we obtain $x/x_{sat}$ = 1.48 ± 0.13 for NaCl and $x/x_{sat}$ = 1.34 ± 0.13 for LiCl (Figure 6b).

These values are consistent with predictions from CNT, assuming sterically hindered homogeneous nucleation of the salt crystal (Theory section): on numerically solving eq 22 for $r_c = r_p$, we obtain the theoretical value for dissolved mole fraction $x_{c,th}$, which should be sufficient for crystallization; we find $x_{c,th}$ = 0.140 for NaCl and $x_{c,th}$ = 0.285 for LiCl for $r_p$ = 1.4 nm, corresponding to supersaturations of 1.408 and 1.176 and vapor activities of 0.230 and 0.022, respectively (blue dots in Figure 6b). These values match well with the experimental values of vapor activity $a_c$ (shaded green region, Figure 6b), suggesting that the closure of the hysteresis loops at $a_c$ is associated with the crystallization of the salt solution.

We note that the values of supersaturation extracted from the experimental data and theoretically predicted by CNT are sensitive to the choice of pore size and wettability; in the SI, we propagate typical uncertainties on pore radius and contact angle to evaluate their impact (Figures S9 and S10). The leading effect is that of pore size; for example, assuming $r_p$ = 1.4 ± 0.2 nm yields uncertainties for $x/x_{sat}$ in the ranges of 1.41 ± 0.32 and 1.34 ± 0.17 for experimental supersaturations of NaCl and LiCl, respectively, and 1.42 ± 0.07 and 1.18 ± 0.03 for theoretical supersaturations of NaCl and LiCl, respectively (SI).

An interesting aspect of CNT is that the second term inside the exponential of the right-hand side of eq 22 incorporates the effect of negative pressure (tension) in inducing crystallization. Tension in the liquid is related to the large capillary pressure of the curved nanomenisci at the solution−vapor interface (Theory section). Including this term reduces the theoretical supersaturation for crystallization by ~6% for NaCl and by ~1% for LiCl. Given our experimental uncertainties, it is, however, difficult to isolate this effect in our data.

Finally, we note that the supersaturations estimated here for NaCl are comparable to recent measurements of crystallization in capillary tubes ($x/x_{sat} \simeq 1.6$ according to several authors[42−44]), where crystal nucleation is expected to be limited by kinetics and not steric confinement as assumed in our CNT model. Other supersaturation estimates range from $x/x_{sat} \approx 1.05-1.1$ in porous media with large pore sizes[45−47] to $x/x_{sat} \simeq 2.3-2.6$ in levitated droplets.[48,49] Further studies are required to identify the relative effects of confinement, heterogeneous nucleation, and kinetics to explain this variability of observed supersaturation.

**Percolation-Induced Optical Scattering.** As discussed in the Theory section, we interpret the maxima in reflectance on the adsorption and desorption isotherms as arising from heterogeneities in the distribution of the liquid and vapor phases within the pores. We observe continuous, unimodal changes in reflectance on both adsorption and desorption branches of Figures 3 and 4. As discussed in the Theory section, we speculate that disordered fluid networks of size comparable to the wavelength of light are formed on both the filling and draining of solution-filled porous media during respectively adsorption and desorption and that this results in enhanced scattering, as observed in our isotherms. Figure 7a presents the hypothetical schematic diagram of filling of the porous network at vapor activities corresponding to maximum scattering on adsorption ($a_{ap}$) and desorption ($a_{dp}$). As discussed earlier in the Theory section, the formation of

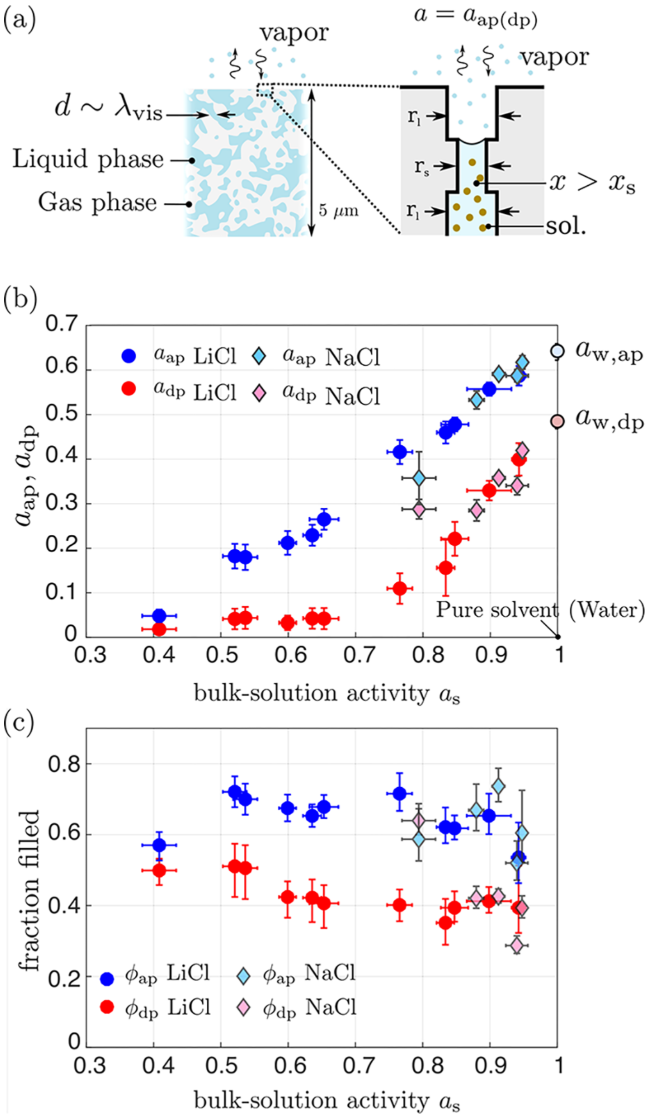

**Figure 7.** Enhanced scattering as a result of the distribution of solution at adsorption-peak ($a_{\mathrm{ap}}$) and desorption-peak ($a_{\mathrm{dp}}$) vapor activity. (a) Schematic diagrams of the hypothetical state of the pore solution at vapor activity $a = a_{\mathrm{ap(dp)}}$, where pore space connectivity and pore size nonuniformity lead to clusters of liquid and gas phases with cluster dimension $d$ on the order of the visible wavelength of light, $\lambda_{\mathrm{vis}}$. The concentration of the pore solution increases as the meniscus recedes with decreasing vapor activity ($x > x_s$); larger pores connected to smaller pores ($r_s < r_l$) remain undrained due to the pore-blocking effect (Theory section). (b) Experimental values of adsorption-peak activity ($a_{\mathrm{ap}}$) and desorption-peak activity ($a_{\mathrm{dp}}$) as a function of bulk-solution activity ($a_s$) for NaCl solution and LiCl solution. (c) Calculated fraction of pore volume filled (based on eq 26), $\phi_{\mathrm{ap}}$ and $\phi_{\mathrm{dp}}$, at vapor activities $a_{\mathrm{ap}}$ and $a_{\mathrm{dp}}$ for LiCl and NaCl solutions, respectively. Error bars for $a_s$, $a_{\mathrm{ap}}$, and $a_{\mathrm{dp}}$ represent the uncertainty in the experimental values extracted from the isotherms.

clusters of liquid and vapor associated with the increase in light scattering results from two underlying causes: the pore size distribution (pore-blocking percolation effect) and continuous changes in the activity or, equivalently, the concentration of the solution (eq 26, Figure 7a).

We observe that adsorption-peak activity, $a_{\mathrm{ap}}$, and desorption-peak activity, $a_{\mathrm{dp}}$, as a function of $a_s$ (Figure 7b) show similar trends for NaCl and LiCl solutions. On the adsorption branch, for vapor activity below $a_{\mathrm{at}}$, a confined solution can be in equilibrium with vapor of higher activity by decreasing its concentration by filling additional pore volume. Similarly, during desorption, a confined solution can be in equilibrium with the vapor by the recession of the pore solution or, in other words, by increasing the concentration.

We used $x_{\mathrm{ap(dp)}}$ calculated from eq 25a and 25b in eq 26 to calculate the fraction of pore volume filled, $\phi_{\mathrm{ap(dp)}}$ (Figure 7c), at the vapor activity of maximum scattering, $a = a_{\mathrm{ap(dp)}}$. Reflectance peaks occur in two distinct ranges of the volume fraction of filled pores. Upon adsorption, the filling fraction, $\phi_{\mathrm{ap}}$, corresponding to vapor activity, $a_{\mathrm{ap}}$, occurs from 0.53 to 0.69 of total pore volume; upon desorption, the filling fraction, $\phi_{\mathrm{dp}}$, corresponding to vapor activity, $a_{\mathrm{dp}}$, occurs from 0.35 to 0.52. Note that these values are the same for both NaCl and LiCl solutions. These results indicate that there is a relatively narrow variation in $\phi_{\mathrm{ap}}$ and $\phi_{\mathrm{dp}}$ for solutions with a wide range of bulk-solution activity, $a_s$, and there are no significant trends in $\phi_{\mathrm{ap}}$ and $\phi_{\mathrm{dp}}$ as a function of $a_s$. Because the filing fraction is not an explicit function of the pore radius, evaluating the effect of pore size distribution on the filling fraction here is nontrivial and requires detailed studies of pore-scale processes in disordered pore networks. The theoretical filling fraction associated with the critical percolation threshold for square and triangular lattices ranges from 0.3 to 0.6.[50] Therefore, the constant filing fractions obtained experimentally at $a_{\mathrm{ap}}$ and $a_{\mathrm{dp}}$ hint at percolation-induced scattering. The fact that these values are also independent of solute suggests that increased scattering is a result of physical formations and is not influenced by the chemical composition of these clusters.

## ■ CONCLUSIONS

We have demonstrated the use of reflectance isotherms to evaluate the thermodynamic state of solutions in equilibrium with subsaturated vapor in mesoporous silicon. This technique could be generalized to other mesoporous materials. We have shown that a modified Kelvin–Laplace equation for solution quantitatively explains the features in the isotherms for pore liquids of various compositions. We have found that the collapse of the hysteresis loop is independent of the activity of bulk solution and well matches the theoretical prediction for the onset of crystallization derived from classical nucleation theory for the suppression of crystallization due to steric hindrance of the critical nucleus by the pores. However, we are uncertain about the mode of nucleation and the role of kinetics in crystallization. Our results also suggest the strongly shifted deliquescence of confined NaCl crystals compared to the bulk. We have shown the existence of reflectance minima (maxima in $\Delta I/I$) upon both adsorption and desorption, which are consistent with invasion percolation resulting in pore-space correlation and pore-blocking-induced scattering. The successful use of bulk properties and thermodynamic arguments to explain these results implies that they remain relevant to strongly confined scenarios (~3 nm).

Reflectance isotherms of mesoporous materials contribute to our fundamental understanding of wetting and drying with nanoconfined solutions. They provide a convenient way to investigate the impact of solutes on sorption dynamics and thermodynamics and estimate the associated stresses generated in the medium. This understanding could improve our comprehension of phenomena of natural and industrial interest such as damage and cracking and could aid the development of technologies involving confined solutions for desalination, water purification, and geological saline buffers.

## ■ ASSOCIATED CONTENT

### Supporting Information

The Supporting Information is available free of charge on the ACS Publications website at DOI: 10.1021/acs.langmuir.8b04307.

> Properties of NaCl and LiCl solution as a function of concentration, derivation of thermodynamic condition for crystallization, and additional reflectance isotherms (PDF)

## ■ AUTHOR INFORMATION

**Corresponding Authors**

*E-mail: olivier.vincent@univ-lyon1.fr.

*E-mail: ads10@cornell.edu.

**ORCID**

Piyush Jain: 0000-0002-2852-5285

Olivier Vincent: 0000-0002-8876-6072

**Present Address**

[‖]University of Lyon, Université Claude Bernard Lyon 1, CNRS, Institut Lumière Matière, F-69622, Villeurbanne, France.

**Notes**

The authors declare no competing financial interest.

## ■ ACKNOWLEDGMENTS

This work was supported by the National Science Foundation (IIP-1500261), the Air Force Office of Scientific Research (FA9550-15-1-0052), and the U.S. Department of Agriculture (2015-67021-22844) and was performed in part at the Cornell NanoScale Facility, a member of the National Nanotechnology Infrastructure Network (National Science Foundation, grant no. ECCS-1542081).

## ■ REFERENCES

(1) Scherer, G. W. Crystallization in pores. *Cem. Concr. Res.* **1999**, *29*, 1347−1358.

(2) Flatt, R. J. Salt damage in porous materials: How high supersaturations are generated. *J. Cryst. Growth* **2002**, *242*, 435−454.

(3) Berkowitz, B. Characterizing flow and transport in factures geological media: A review. *Adv. Water Resour.* **2002**, *25*, 861−884.

(4) Saadatpoor, E.; Bryant, S. L.; Sepehrnoori, K. New trapping mechanism in carbon sequestration. *Transp. Porous Media* **2010**, *82*, 3−17.

(5) Humplik, T.; Lee, J.; O'Hern, S. C.; Fellman, B. A.; Baig, M. A.; Hassan, S. F.; Atieh, M. A.; Rahman, F.; Laoui, T.; Karnik, R.; Wang, E. N. Nanostructured materials for water desalination. *Nanotechnology* **2011**, *22*, 292001.

(6) Selwitz, C.; Doehne, E. The evaluation of crystallization modifiers for controlling salt damage to limestone. *Journal of Cultural Heritage* **2002**, *3*, 205−216.

(7) Ruiz-Agudo, E.; Mees, F.; Jacobs, P.; Rodriguez-Navarro, C. The role of saline solution properties on porous limestone salt weathering by magnesium and sodium sulfates. *Environ. Geol.* **2007**, *52*, 269−276.

(8) McCarthy, K. A.; Johnson, R. L. Transport of volatile organic compounds across the capillary fringe. *Water Resour. Res.* **1993**, *29*, 1675−1683.

(9) Silliman, S. E.; Berkowitz, B.; Simunek, J.; Van Genuchten, M. T. Fluid flow and solute migration within the capillary fringe. *Groundwater* **2002**, *40*, 76−84.

(10) Sghaier, N.; Prat, M.; Nasrallah, S. B. On ions transport during drying in a porous medium. *Transp. Porous Media* **2007**, *67*, 243−274.

(11) Huinink, H. P.; Pel, L.; Michels, M. A. J. How ions distribute in a drying porous medium: A simple model. *Phys. Fluids* **2002**, *14*, 1389−1395.

(12) Schoch, R. B.; Han, J.; Renaud, P. Transport phenomena in nanofluidics. *Rev. Mod. Phys.* **2008**, *80*, 839−883.

(13) Pel, L.; Huinink, H.; Kopinga, K. Ion transport and crystallization in inorganic building materials as studied by nuclear magnetic resonance. *Appl. Phys. Lett.* **2002**, *81*, 2893−2895.

(14) Rijniers, L. A.; Huinink, H. P.; Pel, L.; Kopinga, K. Experimental evidence of crystallization pressure inside porous media. *Phys. Rev. Lett.* **2005**, *94*, 23−26.

(15) Thommes, M. Physical adsorption characterization of nanoporous materials. *Chem. Ing. Tech.* **2010**, *82*, 1059−1073.

(16) Valiullin, R.; Naumov, S.; Galvosas, P.; Kärger, J.; Woo, H.-J.; Porcheron, F.; Monson, P. A. Exploration of molecular dynamics during transient sorption of fluids in mesoporous materials. *Nature* **2006**, *443*, 965−968.

(17) Page, J. H.; Liu, J.; Abeles, B.; Deckman, H. W.; Weitz, D. A. Pore-space correlations in capillary condensation in Vycor. *Phys. Rev. Lett.* **1993**, *71*, 1216−1219.

(18) Soprunyuk, V.; Wallacher, D.; Huber, P.; Knorr, K.; Kityk, A. Freezing and melting of Ar in mesopores studied by optical transmission. *Phys. Rev. B: Condens. Matter Mater. Phys.* **2003**, *67*, 144105.

(19) Evans, R. Fluids adsorbed in narrow pores: Phase equilibria and structure. *J. Phys.: Condens. Matter* **1990**, *2*, 8989−9007.

(20) Vincent, O.; Marguet, B.; Stroock, A. D. Imbibition Triggered by Capillary Condensation in Nanopores. *Langmuir* **2017**, *33*, 1655−1661.

(21) Vincent, O.; Szenicer, A.; Stroock, A. D. Capillarity-driven flows at the continuum limit. *Soft Matter* **2016**, *12*, 6656−6661.

(22) Vitagliano, V.; Lyons, P. A. Diffusion Coefficients for Aqueous Solutions of Sodium Chloride and Barium Chloride. *J. Am. Chem. Soc.* **1956**, *78*, 1549−1552.

(23) Sahimi, M. *Flow and Transport in Porous Media and Fractured Rock*; 2011; p 718.

(24) Huber, P. Soft matter in hard confinement: Phase transition thermodynamics, structure, texture, diffusion and flow in nanoporous media. *J. Phys.: Condens. Matter* **2015**, *27*, 103102.

(25) Bocquet, L.; Charlaix, E. Nanofluidics, from bulk to interfaces. *Chem. Soc. Rev.* **2010**, *39*, 1073−1095.

(26) Wagner, W.; Pruss, A. International Equations for the Saturation Properties of Ordinary Water Substance. Revised According to the International Temperature Scale of 1990. Addendum to J. Phys. Chem. Ref. Data 16, 893 (1987). *J. Phys. Chem. Ref. Data* **1993**, *22*, 783−787.

(27) Vincent, O.; Zhang, J.; Choi, E.; Zhu, S.; Stroock, A. D. How Solutes Modify the Thermodynamics and Dynamics of Filling and Emptying in Extreme Ink-Bottle Pores. *Langmuir* **2019**, DOI: 10.1021/acs.langmuir.8b03494.

(28) Conde, M. R. Properties of aqueous solutions of lithium and calcium chlorides: Formulations for use in air conditioning equipment design. *Int. J. Therm. Sci.* **2004**, *43*, 367−382.

(29) Olynyk, P.; Gordon, A. R. The Vapor Pressure of Aqueous Solutions of Sodium Chloride at 20, 25 and 30° for Concentrations from 2 Molal to Saturation. *J. Am. Chem. Soc.* **1943**, *65*, 224−226.

(30) Fukuta, N. Activation of Atmospheric Particles as Ice Nuclei in Cold and Dry Air. *J. Atmos. Sci.* **1966**, *23*, 741−750.

(31) Espinosa, J. R.; Vega, C.; Valeriani, C.; Sanz, E. The crystal-fluid interfacial free energy and nucleation rate of NaCl from different simulation methods. *J. Chem. Phys.* **2015**, *142*, 194709.

(32) Lanaro, G. *Molecular Simulation of Nucleation and Dissolution of Alkali Halides*. Ph.D. Thesis, 2017.

(33) Volmer, M.; Weber, A. Keimbildung in übersättigten Gebilden. *Z. Phys. Chem.* **1926**, *119U*, 277.

(34) Becker, R.; Döring, W. Kinetische Behandlung der Keimbildung in übersättigten Dämpfen. *Ann. Phys.* **1935**, *416*, 719−752.

(35) Frenkel, J. A. General Theory of Heterophase Fluctuations and Pretransition Phenomena. *J. Chem. Phys.* **1939**, *7*, 538−547.

(36) Derluyn, H. *Salt Transport and Crystallization in Porous Limestone: Neutron-X-ray Imaging and Poromechanical Modeling*; ETH, 2012; p 248.

(37) Potter, R.; Brown, D. L. The volumetric properties of aqueous sodium chloride solution from 0°C to 500°C at pressures up to 2000 bar based on a regression of available data in the literature. *Geological Survey Bulletin* **1977**, *5*, C1−C36.

(38) Hamer, W. J.; Wu, Y. Osmotic Coefficients and Mean Activity Coefficients of Uni-univalent Electrolytes in Water at 25 degrees Celsius. *J. Phys. Chem. Ref. Data* **1972**, *1*, 1047−1100.

(39) Steiger, M. Crystal growth in porous materials - I: The crystallization pressure of large crystals. *J. Cryst. Growth* **2005**, *282*, 455−469.

(40) Liu, H.; Zhang, L.; Seaton, N. A. Analysis of sorption hysteresis in mesoporous solids using a pore network model. *J. Colloid Interface Sci.* **1993**, *156*, 285−293.

(41) Robinson, R. A.; Stokes, R. H. *Electrolyte Soutions*; Dover Publications, 1959.

(42) Desarnaud, J.; Derluyn, H.; Carmeliet, J.; Bonn, D.; Shahidzadeh, N. Metastability limit for the nucleation of NaCl crystals in confinement. *J. Phys. Chem. Lett.* **2014**, *5*, 890−895.

(43) Naillon, A.; Duru, P.; Marcoux, M.; Prat, M. Evaporation with sodium chloride crystallization in a capillary tube. *J. Cryst. Growth* **2015**, *422*, 52−61.

(44) Gupta, S.; Pel, L.; Steiger, M.; Kopinga, K. The effect of ferrocyanide ions on sodium chloride crystallization in salt mixtures. *J. Cryst. Growth* **2015**, *410*, 7−13.

(45) Veran-Tissoires, S.; Prat, M. Evaporation of a sodium chloride solution from a saturated porous medium with efflorescence formation. *J. Fluid Mech.* **2014**, *749*, 701−749.

(46) Noiriel, C.; Renard, F.; Doan, M. L.; Gratier, J. P. Intense fracturing and fracture sealing induced by mineral growth in porous rocks. *Chem. Geol.* **2010**, *269*, 197−209.

(47) Chatterji, S. A discussion of the paper ”Crystallisation in pores” by G.W. Scherer. *Cem. Concr. Res.* **2000**, *30*, 669−671.

(48) Na, H. S.; Arnold, S.; Myerson, A. S. Cluster formation in highly supersaturated solution droplets. *J. Cryst. Growth* **1994**, *139*, 104−112.

(49) Hargreaves, G.; Kwamena, N. O.; Zhang, Y. H.; Butler, J. R.; Rushworth, S.; Clegg, S. L.; Reid, J. P. Measurements of the equilibrium size of supersaturated aqueous sodium chloride droplets at low relative humidity using aerosol optical tweezers and an electrodynamic balance. *J. Phys. Chem. A* **2010**, *114*, 1806−1815.

(50) Stauffer, D.; Aharony, A. *Introduction to Percolation Theory*; 1991; Vol. *1*, p 192.

DOI: 10.1021/acs.langmuir.8b04307
*Langmuir* 2019, 35, 3949−3962